The Journal of Chemical Physics

Broadband visible two-dimensional spectroscopy of molecular dyes

Cite as: J. Chem. Phys. **155**, 034201 (2021); https://doi.org/10.1063/5.0053554
Submitted: 08 April 2021 . Accepted: 25 June 2021 . Published Online: 15 July 2021

Lars Mewes, Rebecca A. Ingle, Andre Al Haddad, and Majed Chergui

The Journal of Chemical Physics ARTICLE scitation.org/journal/jcp

Broadband visible two-dimensional spectroscopy of molecular dyes

Cite as: J. Chem. Phys. 155, 034201 (2021); doi: 10.1063/5.0053554
Submitted: 8 April 2021 • Accepted: 25 June 2021 •
Published Online: 15 July 2021

Lars Mewes,[a),b)] Rebecca A. Ingle,[c)] Andre Al Haddad,[d)] and Majed Chergui[a)]

AFFILIATIONS

Laboratoire de Spectroscopie Ultrarapide and LACUS, Ecole Polytechnique Fédérale de Lausanne, ISIC, FSB-BSP, CH-1015 Lausanne, Switzerland

Note: This paper is part of the JCP Special Topic on Coherent Multidimensional Spectroscopy.
[a)]**Authors to whom correspondence should be addressed:** lars.mewes@tum.de and majed.chergui@epfl.ch
[b)]**Now at:** Dynamische Spektroskopien, Fakultät für Chemie, Technische Universität München, Lichtenbergstr. 4, D-85748 Garching b. München, Germany.
[c)]**Now at:** Department of Chemistry, University College London, 20 Gordon Street, London WC1H 0AJ, United Kingdom.
[d)]**Now at:** Paul Scherrer Institut (PSI), 5232 Villigen PSI, Switzerland.

ABSTRACT

Two-dimensional Fourier transform spectroscopy is a promising technique to study ultrafast molecular dynamics. Similar to transient absorption spectroscopy, a more complete picture of the dynamics requires broadband laser pulses to observe transient changes over a large enough bandwidth, exceeding the inhomogeneous width of electronic transitions, as well as the separation between the electronic or vibronic transitions of interest. Here, we present visible broadband 2D spectra of a series of dye molecules and report vibrational coherences with frequencies up to ~1400 cm^{-1} that were obtained after improvements to our existing two-dimensional Fourier transform setup [Al Haddad *et al.*, Opt. Lett. **40**, 312–315 (2015)]. The experiment uses white light from a hollow core fiber, allowing us to acquire 2D spectra with a bandwidth of 200 nm, in a range between 500 and 800 nm, and with a temporal resolution of 10–15 fs. 2D spectra of nile blue, rhodamine 800, terylene diimide, and pinacyanol iodide show vibronic spectral features with at least one vibrational mode and reveal information about structural motion via coherent oscillations of the 2D signals during the population time. For the case of pinacyanol iodide, these observations are complemented by its Raman spectrum, as well as the calculated Raman activity at the ground- and excited-state geometry.

INTRODUCTION

With the advance of pulsed laser technology and ultrafast optics during recent decades, it has become possible to measure frequency-domain optical signals (such as excitation and/or detection frequencies in time-resolved spectroscopy) interferometrically in the time domain. This has sparked a series of technical developments, of which two-dimensional Fourier transform (2DFT) spectroscopy[1–4] is a successful example. These methods represent short wavelength analogs of two-dimensional nuclear magnetic resonance (NMR) spectroscopy[5] and excitation frequency-resolved extensions to their traditional time-resolved "pump–probe" counterparts.[6] A substantial body of work has exploited the excitation frequency resolution of 2DFT spectroscopy at visible wavelengths to resolve open questions in biophysics, among others, concerning the energy transfer mechanisms in light harvesting complexes,[7] chlorosomes,[8] and the Fenna–Matthews–Olson complex,[9] as well as in supermolecular assemblies[10] and charge-transfer dynamics of molecular dimers.[11] Resolving the excitation frequency dependence of the transient signal has the additional advantage that 2DFT techniques are not limited by the Fourier transform limit (the uncertainty between excitation energy and temporal resolution) and allow the measurement of ultrafast phenomena (with time constants of a few tens of femtoseconds) while retaining the highest possible excitation frequency resolution.[12] This has been proved and implemented to study high frequency molecular vibrations, which play an important role in the reaction mechanism in singlet fission,[13–16] during internal conversion in rhodopsin,[17–19] during energy relaxation in cyanobacterial light harvesting,[20] and in many other processes.[21] Efforts to use 2DFT spectroscopy in the visible region to study smaller molecular

systems, such as donor–acceptor dyads,[22] porphyrins,[23,24] and sensitizer-based charged injection,[25] and fully characterizing population transfer therein are ongoing.[26,27] However, in order to take full advantage of 2DFT spectroscopy, the experimental bandwidth needs to exceed the spectral region of interest, i.e., several optical transitions, which, in the visible region and at room temperature, implies spectral ranges of at least 200–300 nm in the excitation and detection frequency dimension. The difficulty is that broadband visible laser pulses with sufficient energy are not easily generated and the current state of the art for 2DFT spectroscopy is limited to the use of white light spectra from non-collinear optical parametric amplifiers (NOPAs), gas filamentation, or hollow core fibers (HCFs). An exception is the broadband 2D white light spectrometer recently implemented by Mehlenbacher *et al.* that utilizes white light generation by self-phase modulation in YAG crystals[28] and photonic crystal fibers,[29] which is suited for experiments that require low pulse energies and high repetition rates. Out of these techniques, HCFs seem to be most suited for truly broadband 2D spectroscopy, spanning from the ultraviolet to the near-infrared with a single light source, as it has previously been shown that HCF pulses can be compressed using light-field synthesis.[30] This is in comparison to approaches that rely on the combination of several light sources, such as in Ref. 31.

The theory and technical details of 2DFT spectroscopy are described in great detail in the literature,[32–37] and Fig. 1 visualizes the laser pulse sequence (in black) for the most commonly encountered two-dimensional photon echo (2DPE) technique. In essence, the excitation frequency of a sample response is resolved via Fourier transformation (FT) of the coherence time-domain that is created by the coherence time delay τ between the excitation pulses with wave vectors k_1 and k_2. After the population (also evolution, waiting, or relaxation) time delay T, a third laser pulse with wave vector k_3 creates a second coherence within the sample that radiates a signal field in a phase-matched direction $k_{sig} = \pm k_1 \mp k_2 + k_3$, which is heterodyne detected with a co-propagating reference pulse, delayed by t_{LO}, called the local oscillator (LO). When the sample consists of an ensemble of quantum systems, its macroscopic

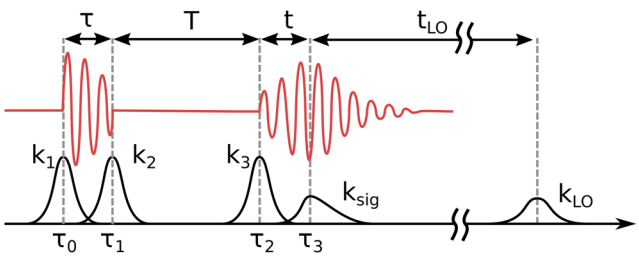

FIG. 1. The interaction of an ensemble of quantum systems with the laser fields k_1, k_2, and k_3 at times τ_0, τ_1, and τ_2 creates a coherence in the density matrix during the coherence time τ and the detection time t, depicted by the oscillation of the red trace, leading to the emission of a photon echo field at time τ_3. This signal k_{sig} is heterodyne detected with a reference field, the local oscillator (k_{LO}), which is delayed by t_{LO}. Prior to the first field interaction and during the population time T, the system's density matrix is typically in a population state, which does not oscillate in time. Since the interaction with the laser field, indicated by the dashed gray lines, can occur at any moment during the pulse envelope, the sample response is convoluted by the laser fields.

polarization, which is responsible for the radiated signal field, is described by a third-order non-linear response function. The latter, in turn, depends on the evolution of the density matrix of the ensemble under the perturbation, i.e., the interaction with the laser pulses, and the behavior of its off-diagonal elements is visualized by the red trace in Fig. 1. Technically, the heterodyne detected signal ($k_{sig} + k_{LO}$) is spectrally resolved (which is the optical analog of the FT: $t \rightarrow \omega_t$) and detected for a series of coherence time delays, which encodes the evolution of the third-order non-linear response function during τ. A subsequent numerical FT along this τ-series yields the excitation frequency dependence of the sample response. Finally, the evolution of this excitation and detection frequency-resolved transient signal during the population time T describes the non-equilibrium dynamics of the ensemble and is comparable to the temporal evolution of a transient absorption (TA) spectrum. These non-equilibrium dynamics are usually differentiated as (i) kinetics due to energy relaxation processes (vibrational relaxation, internal conversion, and intersystem crossing) and (ii) coherences between electronic or vibrational quantum states. In 2DFT spectroscopy, kinetics are observed via the evolution of on-diagonal peaks and off-diagonal cross-peaks, associated with coupling between states and the energy relaxation channels, or reaction pathways, of the system,[26] as well as the broadening of 2D line shapes, which provides information about the interaction between a system and its environment.[38] In visible spectroscopy, coherences involve several electronic and/or vibrational states and are observed as oscillations of the 2D signal during the population time T. While the implications of electronic coherences on the molecular dynamics have been hotly debated,[39–42] vibrational coherences are frequently examined to study dephasing mechanisms due to the environment, as well as relaxation pathways.[18,19,21,43–45] The possibility of studying vibrational coherences has motivated the development of two-dimensional electronic spectroscopy (2DES) with 10 fs, broadband visible laser pulses. The advantage of 2DES is that the origin (ground or excited state) of the observed vibrational coherences can be identified by their excitation and detection frequency dependence in a frequency filtered 2D spectrum, which is obtained via FT of the 2D spectra along the population time, $T \rightarrow \Omega_T$.[10,46–49] Each pattern in such a "beating map" corresponds to a specific combination of non-linear response functions and the experimental data can be interpreted by comparing to beating maps generated from quantum mechanical models.[46,50] An advantage is that such an analysis does not rely on, e.g., fitting of data and the extraction of absolute phase information, and as the interesting quantity is the absolute valued beating map Ω_T, the procedure and interpretation are insensitive to small phase errors of the 2D signal.

The motivation for this work is to assess the applicability of broadband 2DFT spectroscopy in the visible region of the electromagnetic spectrum to study molecular systems with relevance to physical chemistry and we present results on a series of molecular dyes in solution, namely, nile blue (**nb**) perchlorate, rhodamine 800 (**rh800**) perchlorate, terylene diimide (**tdi**), and pinacyanol iodide (**pin**). Their molecular structures are shown in Fig. S1, and their absorption spectra are compared to the white light spectrum of the hollow core fiber (HCF) light source in Fig. S2. A bandwidth of 200 nm, tunable in a range from 500 to 800 nm, allows us to excite several electronic/vibronic transitions coherently and measure their transient evolution with a temporal resolution of <20 fs. This is

validated by the observation of vibrational coherences up to 1400 cm^{-1}, allowing us to extract beating maps for various vibrational modes of the molecules, and demonstrated for the case of **pin**, which serves as an interesting test case due to its light-induced photoisomerization.[51] While comparison to simple theoretical models[46] highlights the information that can be obtained from such an analysis, further work is needed to account for more complex photophysics and experimental considerations, such as non-uniform spectral intensity and finite pulse duration.

EXPERIMENTAL

To achieve the results presented in this work, significant upgrades to a previous version of the experimental setup, described by Al Haddad *et al.* in Ref. 52, have been made. An overview of the current setup is shown in Fig. 2(a). 30 fs laser pulses with a center wavelength of 790 nm and at a repetition rate of 3 kHz are generated by a regenerative amplifier (Coherent Astrella), attenuated to 330 μJ by a combination of a $\lambda/2$ waveplate (HWP) and a transmission polarizer (POL), and focused onto the entrance of an ~1.5 m long, home-built HCF with an inner diameter of 260 μm to generate high-intensity, broadband white light pulses via self-phase modulation.[53,54] The laser focus has a $1/e^2$ diameter of 160 μm, adjustable by an aperture (A) in front of the focusing mirror (FM), for optimal coupling into the HCF.[55–58] The latter is differentially pumped, with 0.5–1 bar of argon at the exit and <10 mbar at the entrance, to avoid instabilities of the white light spectrum due to ionization.[56] The resulting white light spectrum is shown in Fig. 2(b) and spans a wavelength range from 470 to 970 nm with a pulse energy exceeding 180 μJ, corresponding to 65%–70% transmission through the HCF, and an rms noise of 0.3%–0.5%, as measured on a shot-to-shot basis using a photodiode. This is comparable to the 0.2%–0.3% rms noise of the 800 nm fundamental. The HCF output is collimated using a spherical collimation mirror (CM) and

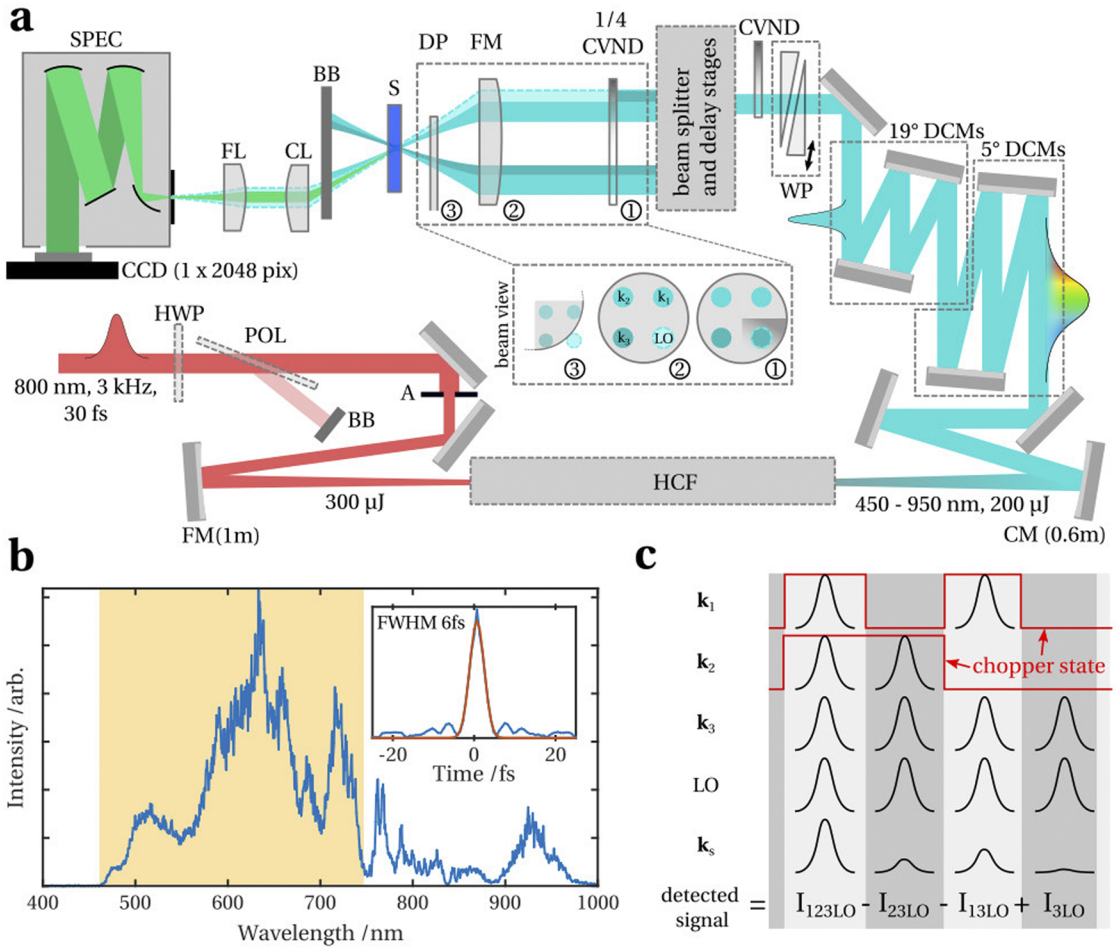

FIG. 2. (a) Schematic overview of the experimental setup. HWP: half-wave plate, POL: polarizer, BB: beam block, A: aperture, FM: focusing mirror, DP: delay plate, HCF: hollow-core fiber, CM: collimating mirror, CMs: chirped mirrors, WP: wedge pair, CVND: circularly variable neutral density filter, S: sample, CL: collimating lens, FL: focusing lens, SPEC: spectrograph, and CCD: charge-coupled device. (b) Fiber white light spectrum with the used spectral region highlighted by the shaded region and its Fourier transform (inset). (c) Two choppers [not shown in (a)] modulate k_1 and k_2 at R/2 and R/4, respectively, and the background is subtracted on a four-shot basis.

the temporal chirp of the white light pulses is canceled out by a set of double-angle dispersion compensated mirrors (DCMs, Ultrafast Innovations, PC70), of which one pair is dichroic in order to suppress wavelengths >800 nm, and fine-tuning of the temporal phase is achieved by changing the optical path through a pair of thin fused silica (Suprasil) wedges (FemtoOptics, OA924). After the wedge pair (WP), the laser beam is split into four identical replicas in the BOXCARS geometry by a combination of beam splitters (Thorlabs, EBS05, custom thickness of 1 mm) and mirrors, which are mounted on stable home-built aluminum mounts to achieve a passive phase-stability of ~λ/60 at λ = 540 nm,[52] highlighted by shot-to-shot interferograms in Fig. S3. For details about the implementation of the beam splitters and interpulse delay generation, see Refs. 52 and 59. Importantly, the pair-wise manipulation of pulses allows us to delay k_{LO} time-synchronously with the photon echo signal and thus acquire the signal in a rotating frame of reference. A 50.8 mm diameter spherical focusing mirror (FM) with a focal length of 1000 mm at normal incidence focuses all four beams to a common focal point (in a folded geometry) with a full width at half maximum (FWHM) diameter of ~300 μm. The long focal length minimizes the angle between beams to <1.6° and thus avoids signal distortions due to spatial filtering.[60] The intensity of all four beams, k_1, k_2, k_3, and k_{LO}, is adjusted by a circular variable neutral density (CVND) filter prior to the beam splitters and k_{LO} is further attenuated by a factor of 10^3–10^4 by a custom-made CVND filter, which is only coated on one-quarter of its surface to attenuate k_{LO}, while keeping the amount of glass equal in all four beam paths. Together with the ~300 μm beam diameter and a typical pulse energy of 100 nJ, the laser fluence at the sample position is 300 μJ/cm^2. By passing k_1–k_3 through a 1 mm fused silica delay plate (DP), k_{LO} precedes k_1, k_2, and k_3 by ~1.5 ps creating the LO delay t_{LO}. The sample (S) is contained inside a cuvette with a path length of 100 μm and ~100 μm thin windows (Starna UTWA/2) to avoid additional group velocity dispersion. After the sample, k_1, k_2, and k_3 are blocked by an aperture/beam block (BB), and the co-propagating signal and LO are collimated and refocused onto the entrance slit of a spectrograph (SPEC, Andor Shamrock 303i) using a pair of lenses for collimation (CL) and focusing (FL). Their spectral interference is recorded shot-to-shot at 3 kHz by a home-built data acquisition board featuring a CCD detector (Hamamatsu S11155-2048-02) in combination with a field-programmable gate array (FPGA) integrated circuit (National Instruments). An accurate wavelength calibration with a resolution of ~0.5 nm is achieved using neon emission lines and the remaining phase error is corrected for by the procedure outlined in Ref. 61, which is important to successfully phase the broadband 2D spectra.[12,62] Background signals that are emitted in the phase-matched direction (i.e., along k_{sig}) are eliminated by mechanically chopping k_1 at half and k_2 at one-quarter of the laser repetition rate, and subtracting the different combinations on a four-shot basis according to the acquisition scheme, as shown in Fig. 2(c). With the background subtracted, the interference between the signal and the LO is averaged over 1000–2000 acquisitions to increase the signal-to-noise ratio. Transient grating (TG) frequency-resolved optical gating (FROG)[63] within a 100 μm thin cuvette filled with spectroscopic grade ethanol (Sigma-Aldrich) is used *in situ* to determine an instrument response function (IRF) of 10–15 fs, as shown in Fig. 3(a), and an exemplary dataset $I(\tau, T, \omega_t)$ of the interference between photon echo signals from **pin** with the LO for a single coherence time scan is shown in Fig. 3(b) (with the full detection frequency range displayed in the inset). Since k_{LO} changes time-synchronously with the photon echo, the signal is slowly varying in τ, i.e., the measurement is performed in a rotating frame of reference. To eliminate spectral fringes due to the interference of unwanted scattered light, e.g., from dust particles inside the sample cell, with the LO, a combination of fast and slow linear stages is used to randomly move the sample cuvette side-to-side, perpendicular to the direction of the laser beams. This changes the phase of the scattered light at random during the data averaging and thus decreases the visibility of unwanted spectral interference fringes, while leaving the spectral phase of the interference between the signal and LO unchanged. The raw data $I(\tau, T, \omega_t)$ is Fourier-filtered using a square windowing function in the t-domain centered at t_{LO}, resulting in the complex dataset $C(\tau, T, \omega_t)$. $C(\tau, T, \omega_t)$ is then multiplied with a phase function, whose parameters are found by comparison with broadband TA measurements,[3,12] and Fourier-transformed along the τ-domain to yield absorptive 2D spectra $I(\omega_\tau, T, \omega_t)$. Beating maps are extracted from $I(\omega_\tau, T, \omega_t)$ by binning $I(\omega_\tau, T, \omega_t)$ in ω_τ and ω_t to increase the computational speed, fitting individual T-domain signals (i.e., for each ω_τ/ω_t bin) with a convolution of Gaussian IRF- and exponential functions, and Fourier transformation $T \rightarrow \Omega_T$ to yield $I(\omega_\tau, \Omega_T, \omega_t)$ spectra. The data are zeropadded prior to Fourier transformation to increase the Ω_T resolution, but we refrain from

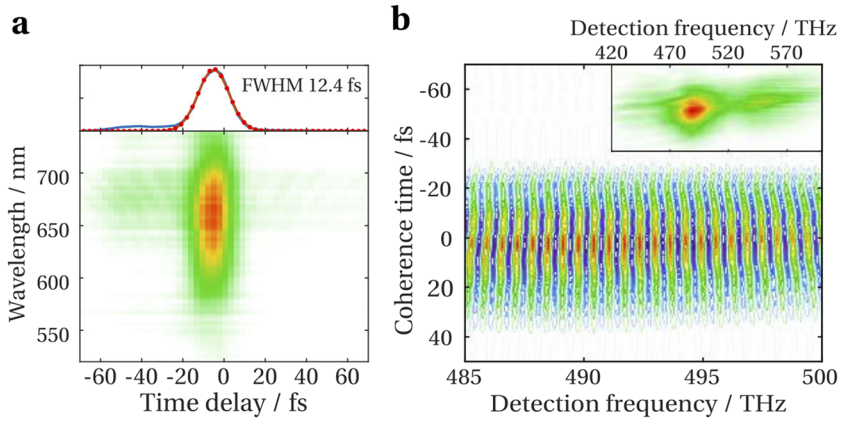

FIG. 3. (a) Typical transient grating FROG measurement of ethanol inside a 100 μm cuvette with thin windows showing that the instrument response function has a temporal duration of <15 fs and spans ~200 nm. The time zero offset is non-representative and has been adjusting prior to 2D measurements. (b) The interference fringes of the interferometrically detected photon echo signal of **pin** contain the linear phase of the temporal delay between the signal and the LO, as well as the phase of the photon echo signal and (inset) the full data spans ~180 THz (~200 nm) in the visible.

applying Fourier-filtering techniques, in order to not introduce artifacts during the data processing.

Auxiliary TA spectra are measured *in situ* and under identical experimental conditions of the white light spectrum and of its compression by blocking k_1 and k_3. The population time delay T then controls the delay between the pump pulse k_2 and the probe pulse k_{LO} and pump–probe spectra are calculated according to $\Delta OD \approx \frac{1}{\ln(10)} \frac{I_p - I_u}{I_u}$. Here, I_p and I_u are the intensities of the probe spectrum, when the sample was pumped (p) or unpumped (u), respectively. Interference fringes from scattered broadband pump pulses are reduced by randomly moving the sample sideways (*vide supra*) and removed completely from the TA data by Fourier filtering in the detection frequency-domain. The TA data are then used to phase the complex 2D data and extract absorptive 2D spectra, according to the projection-slice theorem.[12,62]

The molecular dyes **nb** (Sigma-Aldrich), **rh800** (Sigma-Aldrich), and **tdi** (KU dyes) are used as received and dissolved in spectroscopic grade ethanol, and **pin** (Sigma-Aldrich) is dissolved in spectroscopic grade methanol. The sample concentration is adjusted to an optical density of 0.15–0.3 at the peak wavelength (in the visible region) inside a 100 μm cuvette with ~100 μm thin windows (Starna UTWA/2) to allow for sufficiently strong 2D and TA signals. Absorption spectra of the molecular dyes are measured on a Shimadzu UV-3600 UV–vis spectrometer. Raman spectra were acquired on a Renishaw inVia Raman Microscope (resolution: 1–2 cm^{-1}) with an excitation wavelength of 532 or 785 nm, as indicated in the text. As the dye molecules strongly fluoresce, Raman spectra are recorded under pre-resonant conditions[64] and fluorescence background signals are subtracted from the data. For pin, Raman activities and frequencies were calculated at the optimized ground [DFT/M06-2X/6-311g(d,p)] and excited state [LR-TDDFT/TDA/M06-2X/6-311g(d,p)] geometries. All frequencies are reported with a 0.97 scaling factor applied.[65,66]

RESULTS AND DISCUSSION

Development of an optimal 2DFT experiment for studying photoinduced processes of molecular systems at room temperature requires consideration of various experimental factors. Typical spectral observables are inhomogeneously broadened and the gap between different electronic or vibronic states is on the order of 0.1–1 eV, as molecules that absorb visible light have extended, conjugated π-systems and are composed of many atoms, leading to a manifold of electronic states and a high number of vibrational levels. Non-radiative relaxation processes between these closely spaced states/levels often occur on extremely short timescales,[67,68] requiring simultaneous time and energy resolution to distinguish their spectroscopic signals.

In the following, we outline how these experimental factors are tackled by broadband 2DFT spectroscopy, demonstrated through the observation of several vibronic spectral features, as well as vibrational coherences up to ~1400 cm^{-1} during the evolution time, for **tdi**, **pin**, and **rh800**. Focusing on **nb** and **pin**, we show how the quality of the vibrationally resolved data can be used to investigate the connection between structural and electronic degrees of freedom through analysis of the excitation and detection frequency dependence of vibrational coherences.[48,50] However, first, to quantify and evaluate the performance of the experiment, specifically its bandwidth and simultaneous temporal and spectral resolution, we present the absorptive 2D spectra for **tdi**, **pin**, and **rh800** at T ≈ 100 fs, which have been obtained under identical experimental conditions (white light spectrum, compression, alignment), in Figs. 4(a)–4(c). All 2D spectra are plotted with the excitation frequency ω_τ on the x axis and the detection-frequency ω_t on the y axis, and positive signals correspond to the ground state bleach (GSB) and stimulated emission (SE), while negative signals originate from the excited state absorption (ESA). In the 2D spectrum, the on-diagonal signal corresponds to the linear absorption spectrum, which is evident when comparing the 2D spectra in Figs. 4(a)–4(c) with their respective steady-state absorption (red plots on the ω_τ-axis). Their photophysical behavior can be described using a displaced oscillator (DO) model, where the two lowest-lying absorption bands correspond to the $v'' = 0 \rightarrow v' = 0$ and $v'' = 0 \rightarrow v' = 1$ bands of the molecule's vibronic progression.[50] Here, v'' is the vibrational level of the ground and v' is the vibrational level of the excited state. The steady-state absorption spectra of **tdi** and **rh800** show a third vibronic band of the $v'' = 0 \rightarrow v' = 2$ transition at 18 000 and 17 500 cm^{-1}, respectively. In the 2D spectra, the vibronic progression for **tdi**, **pin,** and **rh800** manifests itself as a square pattern with two on-diagonal and two off-diagonal GSB peaks, since, quite intuitively, excitation of one vibronic transition will also bleach the other(s) due to the common ground state. In addition to the GSB, the 2D spectra contain the SE, which, after vibrational relaxation, exhibits vibronic transitions originating mainly from $v' = 0$ into the $v'' = 0, 1, 2, \ldots$, vibrational manifold of the ground state.[50,69] These signals are red-shifted from the excited transitions by 0, 1, 2, . . ., vibrational quanta, depending on the initially excited vibronic transition, as well as by the Stokes shift. To highlight the difference between GSB and SE, Fig. S4 shows the decomposition of the calculated 2D spectrum of a DO model with two electronic levels into its components.[70,71] The 2D spectrum of **rh800** in Fig. 4(c) features an additional negative ESA contribution at $\omega_t > 16\,500$ cm^{-1}, coinciding with the ESA band observed in the TA spectrum (black plot). This can be modeled by introducing a third electronic level in the DO model, as illustrated in Fig. S5. The decomposition of this three-level DO model shows that ESA can potentially overlap with GSB and SE signals, depending on the energetics of the system. Thus, it is reasonable to assume that the 2D spectra of **tdi** and **pin** also contain a contribution from the ESA, which manifests itself as a diminution of the positive GSB and SE signal, rather than a negative contribution, which might still be present at $\omega_t > 18\,500$ cm^{-1}, i.e., outside of the observable spectral region of our experiment. Overall, the 2D spectra of **pin** and **tdi** in Figs. 4(a) and 4(b) correspond well to recently published data,[69] while, to the best of our knowledge, no literature 2D spectrum for **rh800** is available. During the first picosecond of the population time T, neither the transient signal of **tdi** [Figs. 4(a) and 4(d)], nor that of **rh800** [Figs. 4(c) and 4(f)] decays, in agreement with the long life times of their excited states.[72,73] The observed vibrational coherences [Figs. 4(d) and 4(f)] with frequencies of $\Omega_T < 600$ cm^{-1} [Figs. 4(g) and 4(i)] are related to the torsional motions and skeletal vibration of the molecules,[74] and for **rh800,** they agree, within the experimental error, with those observed in three-pulse photon echo peak shift experiments.[75] The 2D signal of **pin** in Fig. 4(b) exhibits oscillations up to $\Omega_T \approx 1400$ cm^{-1} [Fig. 4(h)], in addition to an exponential decay (Fig. S6) that is associated with

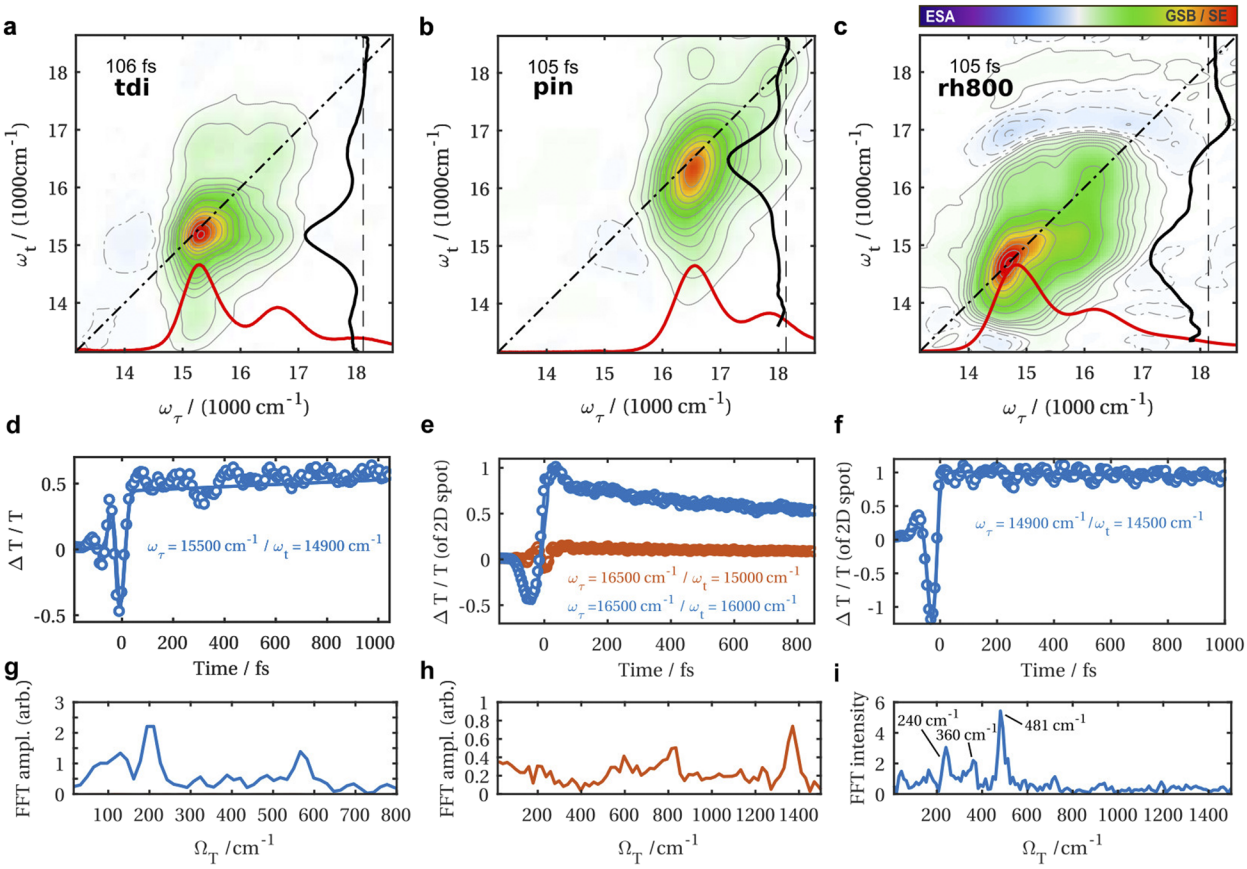

FIG. 4. 2D spectra of (a) **tdi**, (b) **pin**, and (c) **rh800** at ~100 fs with contour lines at ±1, 4, 8, 12, 16, 20, 40, . . ., % of the maximum absolute signal after T ≈ 20 fs. The corresponding absorption and transient absorption spectra are plotted in red and black on the ω_τ- and ω_t-axis, respectively. The time traces (d)–(f) and the Fourier transform spectra of their residuals (g)–(i) exemplify the obtainable information content.

the 5.2 ± 0.3 ps isomerization timescale of the central C=C double bond, highlighted in red in Fig. 5(a), of the methine backbone.[76] This photoisomerization involves an overdamped wavepacket motion[77] along a combined stretching and torsion reaction coordinate of the methine C=C backbone double bond.[51] The two most prominent vibrational coherences observed in the 2D signal of **pin**, with 833 and 1360 cm^{-1}, shown in Fig. 5(b) fall within the so-called "fingerprint" region,[74,78–81] indicating that they are highly sensitive to the molecular structure.[74] These modes have been tentatively identified as vibrational normal modes of the methine backbone and are notably distinct from the 1270 cm^{-1} vibrational mode, attributed to a N–C bond of the quinolone groups, that couples to the electronic transition and results in the vibronic splitting of the $\pi \rightarrow \pi^*$ absorption band.[82] *Ab initio* calculations at the M06-2X/6-311g(d,p) level of theory show that the mode at 845 cm^{-1} is dominated by an out-of-plane C–H wag on the methine bridge and the intense mode at 1371 cm^{-1} involves predominantly an in-plane C–H wag on the methine bridge and in-plane distortion of the ring system. The Raman spectra and relevant modes are visualized in Figs. S7 and S8, respectively. While the calculations neglect vibronic effects, the mode at 845 cm^{-1} is likely enhanced by intensity borrowing, as the electronic energies are strongly affected by distortions along its coordinate, which coincides with that of the isomerization reaction.[12] Figure 5(b) shows the Raman spectrum of **pin** in methanol, as well as the frequency spectrum obtained by FT of the evolution time (T → Ω_T) and summation over ω_τ and ω_t. The two vibrational modes at 833 and 1360 cm^{-1} are highlighted in green and orange and the few hundred femtosecond dephasing times of these vibrational modes are reflected in their peak widths. It has previously been shown that beating maps of the rephasing and non-rephasing (NR) parts of the 2D signal at a certain Ω_T can be used to identify whether an observed signal coherence originates from a ground or excited state vibrational coherence.[50] For **pin**, the rephasing and non-rephasing beating maps of the 833 cm^{-1} mode are shown in Figs. 5(c) and 5(d) and those of the 1360 cm^{-1} mode are shown in Figs. 5(e) and 5(f). Overlaid on each beating map are the contour lines of the absorptive 2D spectrum. The non-rephasing beating map of the 833 cm^{-1} mode shows a strong resemblance to the theoretically expected pattern for a SE coherence (inset), while the rephasing beating map of the 1360 cm^{-1} coherence is strongly reminiscent of a GSB coherence. Both models assume a system of DOs. The remaining two beating maps (rephasing of the 833 cm^{-1} coherence and

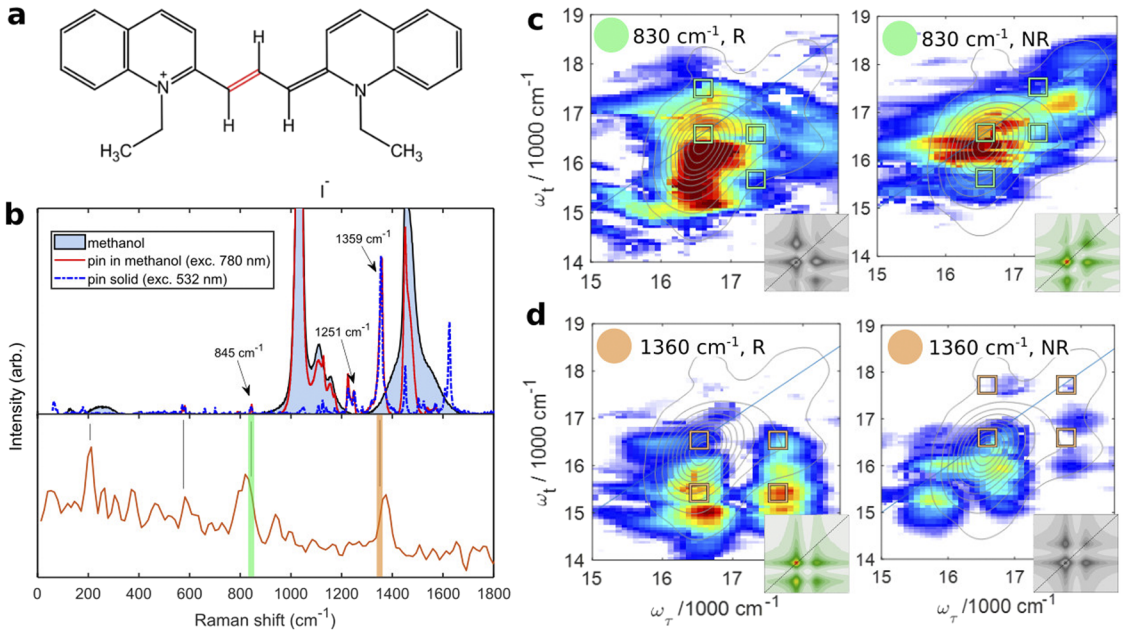

FIG. 5. Fourier transform analysis of **pin** in methanol. (a) Upon $\pi \rightarrow \pi^*$ excitation, the molecule undergoes a cis–trans isomerization around the C=C double bond (red) of the methine backbone. (b) (Top panel) The Raman spectrum of **pin** shows the Raman-active vibrational modes of **pin** (dissolved in methanol and in the solid form) and of methanol. The missing methanol contribution to the Raman spectrum of **pin** dissolved in methanol (most notably in the 1400–1600 cm^{-1} region) is due to the background subtraction, since the solvent is recorded under non-resonant conditions and the pin Raman is resonantly enhanced and a strong fluorescent background is subtracted. (Bottom panel) The Fourier transform ($T \rightarrow \Omega_T$) summed over the ω_τ and ω_t dimensions of the 2D spectrum shows the different frequencies contained within the full 2D dataset. Two Raman-active modes with frequencies of 830 and 1360 cm^{-1} are highlighted in green and orange and, according to Refs. 82 and 98, these correspond to motions of the methine backbone. (c) Beating maps at Ω_T = 830 cm^{-1} of the rephasing (R) and non-rephasing (NR) parts of the 2D signal show the Fourier transform amplitude distribution across the 2D spectrum. Comparison to those calculated for a displaced oscillator (DO) model (insets) shows that, while the non-rephasing beating map seems to agree with that of the stimulated emission component from the DO model, the rephasing beating map is not described by the model and the modeled 2D amplitude distribution is grayed-out to highlight this fact. (d) Analogous to panel (c), however, the rephasing beating map agrees with the model for a ground-state bleach coherence, while the non-rephasing part deviates from the model spectrum. Spectral positions for expected beating peaks are indicated in (c) and (d) by squares as a guide to the eye. For more details about the beating map patterns, see Ref. 50.

non-rephasing of the 1360 cm^{-1} coherence) do not agree with the simulated patterns (the model beating maps are grayed-out to highlight this fact), suggesting that the behavior of the system differs from the idealized DO. This is a reasonable assumption, considering that immediately after optical excitation, the system evolves away from the Franck–Condon region and toward a conical intersection along a combination of normal coordinates. Furthermore, the amplitudes of diagonal and off-diagonal oscillatory features depend on the displacement between the ground- and excited state potential energy surfaces.[50] For example, for a Huang–Rhys factor of 1, the amplitudes of the diagonal oscillatory features (peaks in the beating map) vanish for the rephasing case, while they remain in the non-rephasing data. The precise interpretation of the beatings maps is, however, complicated by different experimental effects. These include (i) the finite laser pulse duration, which effectively suppresses high frequency coherences,[18] potentially leading to the equal intensity of the coherences observed at 833 and 1360 cm^{-1}, as exemplified in Fig. S9; (ii) diminution/amplification of spectral features due to the inhomogeneous white light spectral intensity. For example, for typical HCF white light spectra [see Fig. 3(b)] with decreasing intensity for increasing wavelengths, this can lead to the suppression of signal intensities (kinetics and coherences alike) at higher ω_τ and ω_t; (iii) ESA contributions that cannot be distinguished due to overlap with the observed GSB and SE, resulting in the presence of vibrational coherences encoded in the ESA evolution. These might obscure the expected beating map patterns and are not taken into account using a two-level DO model. Despite these considerations, we note that the coherences with Ω_T = 833 and 1360 cm^{-1} clearly correspond to the vibrations observed in the Raman spectrum and understanding their excitation and detection frequency dependence, possibly via more elaborated modeling[83–85] convoluted with experimental parameters (such as the white light spectrum), might yield additional mechanistic insight into the **pin** photoisomerization.

For the case of **nb**, which does not exhibit distinct bands in the absorption spectrum, the observed 2D spectrum agrees reasonably well with previously published data.[86] At a population time of T = 100 fs, shown in Fig. 6(a), its shape is broad, featureless, and slightly elongated along the diagonal, consistent with the absorption- (red plot) and the TA spectrum (black plot). The line shape can be explained by inhomogeneous broadening, the large number of vibrational modes that couple to the electronic transition at room temperature,[86] and the presence of a broad and red-shifted SE signal that coalesces with the GSB. During the first picosecond of

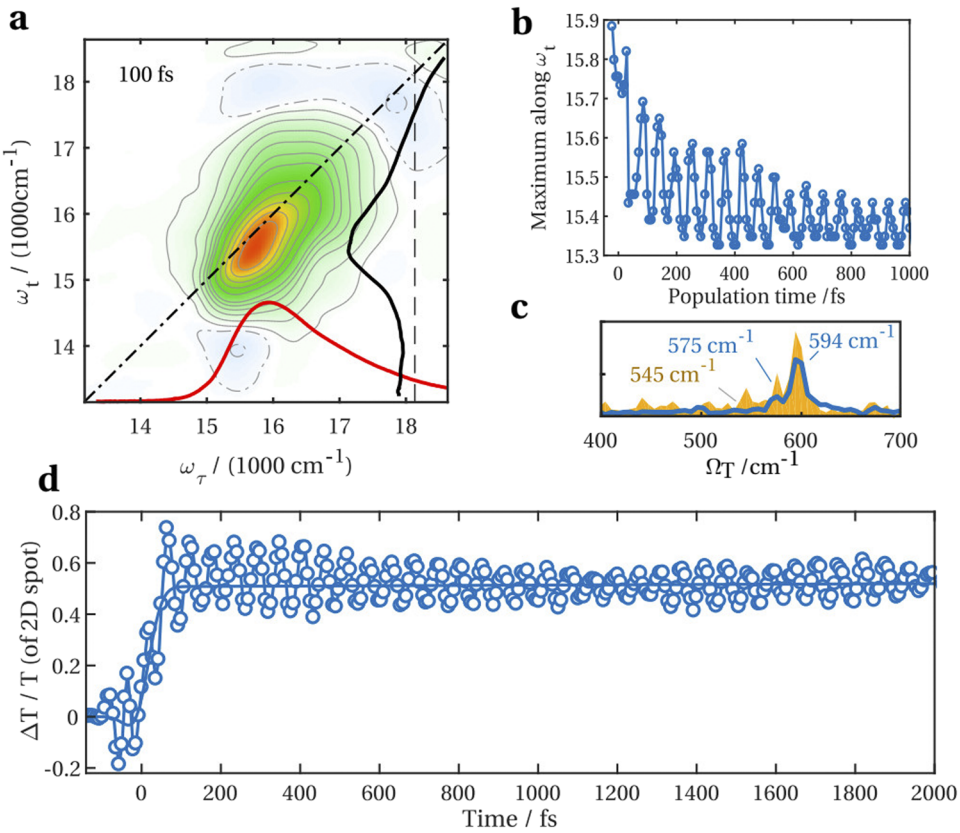

FIG. 6. (a) The 2D spectrum of **nb** at ~100 fs with contour lines at ±1, 4, 8, 12, 16, 20, 40, . . ., % of the maximum signal is compared with the absorption and transient absorption, shown as red and black plots. (b) The peak position shifts to lower ω_t over time, due to the Stokes shift, and both the peak position and (d) the time trace at ω_τ; ω_t = 15 800 and 15 000 cm^{-1} oscillate during the population time T. (c) The Ω_T frequency spectrum of the time trace is displayed in (d) in blue and the frequency spectrum summed over ω_τ and ω_t in yellow.

the population dynamics, the peak in the 2D spectrum shifts to lower energies due to the dynamic Stokes shift, as observed by the temporal evolution of the peak position along ω_t in Fig. 6(b) (blue plot). An exponential fit shown in Fig. S10 reveals a fast time constant of 135 fs, as well as a slow one with small amplitude that is obscured by the vibrational coherence. Beyond 1 ps, it remains located ~450 cm^{-1} below the diagonal, which is ~60% of the 780 cm^{-1} Stokes shift of **nb** in ethanol.[87] Both the peak position along ω_t and the 2D signal intensity at ω_τ, ω_t = 15 000 and 16 000 cm^{-1}, shown in Fig. 6(c), are strongly modulated by vibrational coherences, the most prominent of which, with Ω_T = 594 cm^{-1}, has previously been reported[86,88–92] and assigned to a ring-breathing mode[86] or an in-plane bending- and ring-deformation mode of **nb**.[93,94] Its intensity is explained by the enhanced polarizability along the coordinate of the vibrational mode, according to resonance Raman theory,[95] and the destructive interference with the Ω_T = 575 cm^{-1} vibrational mode at T ≈ 1200 fs has previously been observed in Refs. 93 and 96. Interestingly, to reproduce the node at T ≈ 1200 fs, the relative phase between the two underlying vibrational modes with Ω_T = 575 cm^{-1} and Ω_T = 594 cm^{-1} must be shifted by $\pi/2$, as illustrated in Fig. S11. This phase shift might be due to the fact that the interfering wavepackets propagate on different, e.g., the ground- and excited state, potential energy surfaces. Additional support for this hypothesis comes from the fact that the excitation is of π–π^* character and thus softens the central ring system of **nb**, leading to a frequency downshift of the associated vibrational modes.[97] With sufficient knowledge of the potential energy landscape, this phase difference might be used to obtain a more detailed picture of the **nb** potential energy surfaces. Finally, the ESA of **nb** appears at ωt > 17 500 cm^{-1} in the 2D spectrum, as well as the TA spectrum (black plot in Fig. 5), similar to early 2D spectra published by Brixner *et al.* in Ref. 1.

CONCLUSION AND OUTLOOK

By characterizing a series of molecular dyes, we demonstrate the capabilities of our upgraded 2DPE setup with the following key characteristics: (i) a hollow core fiber white light with the Gaussian beam profile and 200 nm usable bandwidth between 500 and 800 nm (ii) compressed to a sub-20 fs pulse duration using a chirped mirror compressor is (iii) split using a beam splitter-based BOXCARS geometry, allowing for (iv) 2D measurements in a rotating frame of reference with (v) shot-to-shot detection at 3 kHz and (vi) an acquisition time of <1 min per 2D spectrum. (vii) Auxiliary

TA spectra can be acquired under identical experimental conditions. This allows for the routine measurement of molecular systems with spectrally broad transitions in the visible. The beam quality, repetition rate, energy, and spectrum are ideally suited for time-resolved spectroscopy and the chirped mirror compressor proved to simplify compression of the laser pulse to below 20 fs. Measuring in a background-free BOXCARS geometry has the advantage that even small third-order signals can be measured by adjusting the LO separately and allows the straight-forward extraction of rephasing and non-rephasing signal components, both of which are not easily achieved using a pump–probe geometry for 2D spectra. Rotating frame and shot-to-shot detection are of advantage for data acquisition, noise removal, and data reconstruction, and the possibility to measure TA, using the LO as a probe, allows us to obtain vital auxiliary information for phasing of the complex 2D dataset.

The results presented in this article highlight the capability of the experimental setup to measure 2D spectra with a bandwidth exceeding the width of the vibronically split molecular absorption bands. All dyes display the 2D spectra characteristic of DOs, as well as a rich series of vibrational coherences during the population time T. The most prominent coherences in **pin**, with 833 cm^{-1} and with 1360 cm^{-1}, likely correspond to modes associated with methine backbone distortions[98] and are thus involved in the photoisomerization of the molecule. Beating maps point toward their different microscopic origin and show a complicated dependence on the excitation and detection frequencies due to experimental considerations, as well as the properties and photophysical behavior of **pin**. Quantum mechanical models have previously been shown to provide valuable information for interpreting simple 2D spectra, and we expect that more rigorous modeling that potentially includes experimental parameters, such as the employed laser spectrum, will allow us to extract further information about the dynamics of the pin photoisomerization. For **nb**, the vibrational coherences exhibit beatings between different modes, which can also provide structural information on the geometry of the molecule, and, by extension, information on its electronic state.

In general, the observation of coherences in broadband visible 2D spectroscopy allows us to study the influence of structural dynamics onto the electronic relaxation mechanisms in complex molecular systems, such as sensitizing dyes for solar cell applications, the Q-bands of porphyrins and porphyrin assemblies, and photoswitches via their excitation and detection frequency-dependence. This is possible in the visible spectral region >480 nm with existing HCF,[52,99,100] NOPA,[38,69,101] gas filamentation,[102] crystal,[103] and photonic crystal fiber[29] white light sources and possibly between 350 and 500 nm, as well as in the UV, using achromatic second harmonic generation.[104–106]

SUPPLEMENTARY MATERIAL

See the supplementary material for molecular structures; absorption spectra compared to the HCF white light spectrum; calculated 2D spectra for a displaced oscillator model with two and three electronic levels and one vibrational level showing the absorptive as well as the GSB, SE, and ESA component; Raman spectra of **pin** compared predictions for *ab initio* quantum mechanics for the optimized ground- and excited-state minimum geometries; vibrational normal for **pin** on the S_0 state and corresponding to the 845 and 1360 cm^{-1} mode; as well as the laser pulse length dependence of high frequency components in the 2D data.

ACKNOWLEDGMENTS

This work was supported by the Swiss National Science Foundation (SNSF) via the National Centre of Competence in Research: Molecular Ultrafast Science and Technology (NCCR:MUST) and Project No. P2ELP2_187957. The authors would like to acknowledge the work of the EPFL ISIC electronic and mechanical workshops for the development of the CCD detector used in the 2D setup and the help with various mechanical components. The authors also like to thank Andrea Abram (Professor A. G. Köhler) and the Catalysis Research Center (CRC) at the Technical University of Munich for providing the Raman spectra.

DATA AVAILABILITY

The software module to simulate 2D spectra of displaced oscillators was written by L.M. and is based on the QuantumOptics.jl (https://qojulia.org/) package in Julia (https://julialang.org/). The code can be found at https://github.com/lbmnky/MultidimensionalSpectroscopy.jl, and L.M. welcomes contributions to its development.

REFERENCES

[1] T. Brixner, I. V. Stiopkin, and G. R. Fleming, "Tunable two-dimensional femtosecond spectroscopy," Opt. Lett. **29**, 884 (2004).
[2] N. Belabas and M. Joffre, "Visible–infrared two-dimensional Fourier-transform spectroscopy," Opt. Lett. **27**, 2043 (2002).
[3] J. D. Hybl, A. Albrecht Ferro, and D. M. Jonas, "Two-dimensional Fourier transform electronic spectroscopy," J. Chem. Phys. **115**, 6606–6622 (2001).
[4] V. I. Prokhorenko, A. Halpin, and R. J. D. Miller, "Coherently-controlled two-dimensional photon echo electronic spectroscopy," Opt. Express **17**, 9764–9779 (2009).
[5] W. P. Aue, E. Bartholdi, and R. R. Ernst, "Two-dimensional spectroscopy. Application to nuclear magnetic resonance," J. Chem. Phys. **64**, 2229–2246 (1976).
[6] C. Ruckebusch, M. Sliwa, P. Pernot, A. de Juan, and R. Tauler, "Comprehensive data analysis of femtosecond transient absorption spectra: A review," J. Photochem. Photobiol., C **13**, 1–27 (2012).
[7] D. Zigmantas, E. L. Read, T. Mancal, T. Brixner, A. T. Gardiner, R. J. Cogdell, and G. R. Fleming, "Two-dimensional electronic spectroscopy of the B800–B820 light-harvesting complex," Proc. Natl. Acad. Sci. U. S. A. **103**, 12672–12677 (2006).
[8] J. Dostál, T. Mančal, R.-n. Augulis, F. Vácha, J. Pšenčík, and D. Zigmantas, "Two-dimensional electronic spectroscopy reveals ultrafast energy diffusion in chlorosomes," J. Am. Chem. Soc. **134**, 11611–11617 (2012).
[9] E. Thyrhaug, R. Tempelaar, M. Alcocer, K. Žídek, D. Bína, J. Knoester, T. L. C. Jansen, and D. Zigmantas, "Unravelling coherences in the FMO complex," arXiv:1709.00318 (2017).
[10] V. Butkus, J. Alster, E. Bašinskaitė, R. Augulis, P. Neuhaus, L. Valkunas, H. L. Anderson, D. Abramavicius, and D. Zigmantas, "Diversity of coherences and origin of electronic transitions of supermolecular nanoring," arXiv:1503.00870 (2015).
[11] O. Bixner, V. Lukeš, T. Mančal, J. Hauer, F. Milota, M. Fischer, I. Pugliesi, M. Bradler, W. Schmid, E. Riedle *et al.*, "Ultrafast photo-induced charge transfer unveiled by two-dimensional electronic spectroscopy," J. Chem. Phys. **136**, 204503 (2012).
[12] D. M. Jonas, "Two-dimensional femtosecond spectroscopy," Annu. Rev. Phys. Chem. **54**, 425–463 (2003).

[13]S. Ito, T. Nagami, and M. Nakano, "Density analysis of intra- and intermolecular vibronic couplings toward bath engineering for singlet fission," J. Phys. Chem. Lett. **6**, 4972–4977 (2015).
[14]A. A. Bakulin, S. E. Morgan, T. B. Kehoe, M. W. B. Wilson, A. W. Chin, D. Zigmantas, D. Egorova, and A. Rao, "Real-time observation of multiexcitonic states in ultrafast singlet fission using coherent 2D electronic spectroscopy," Nat. Chem. **8**, 16–23 (2016).
[15]R. Tempelaar and D. R. Reichman, "Vibronic exciton theory of singlet fission. II. Two-dimensional spectroscopic detection of the correlated triplet pair state," J. Chem. Phys. **146**, 174704 (2017).
[16]Y. Fujihashi, L. Chen, A. Ishizaki, J. Wang, and Y. Zhao, "Effect of high-frequency modes on singlet fission dynamics," J. Chem. Phys. **146**, 044101 (2017).
[17]P. J. M. Johnson, A. Halpin, T. Morizumi, V. I. Prokhorenko, O. P. Ernst, and R. J. D. Miller, "Local vibrational coherences drive the primary photochemistry of vision," Nat. Chem. **7**, 980–986 (2015).
[18]M. Liebel, C. Schnedermann, T. Wende, and P. Kukura, "Principles and applications of broadband impulsive vibrational spectroscopy," J. Phys. Chem. A **119**, 9506–9517 (2015).
[19]C. Schnedermann, M. Liebel, and P. Kukura, "Mode-specificity of vibrationally coherent internal conversion in rhodopsin during the primary visual event," J. Am. Chem. Soc. **137**, 2886–2891 (2015).
[20]J. M. Womick, B. A. West, N. F. Scherer, and A. M. Moran, "Vibronic effects in the spectroscopy and dynamics of *C*-phycocyanin," J. Phys. B: At., Mol. Opt. Phys. **45**, 154016 (2012).
[21]D. M. Jonas, "Vibrational and nonadiabatic coherence in 2D electronic spectroscopy, the Jahn–Teller effect, and energy transfer," Annu. Rev. Phys. Chem. **69**, 327–352 (2018).
[22]I. Pugliesi, H. Langhals, H. Kauffmann, and E. Riedle, "New perspectives on ultrafast Förster resonant energy transfer," EPJ Web Conf. **41**, 05015 (2013).
[23]F. V. A. Camargo, H. L. Anderson, S. R. Meech, and I. A. Heisler, "Time-resolved twisting dynamics in a porphyrin dimer characterized by two-dimensional electronic spectroscopy," J. Phys. Chem. B **119**, 14660–14667 (2015).
[24]F. V. A. Camargo, C. R. Hall, H. L. Anderson, S. R. Meech, and I. A. Heisler, "Time resolved structural dynamics of butadiyne-linked porphyrin dimers," Struct. Dyn. **3**, 023608 (2016).
[25]W. Xiong, J. E. Laaser, P. Paoprasert, R. A. Franking, R. J. Hamers, P. Gopalan, and M. T. Zanni, "Transient 2D IR spectroscopy of charge injection in dye-sensitized nanocrystalline thin films," J. Am. Chem. Soc. **131**, 18040–18041 (2009).
[26]J. Dostál, B. Benešová, and T. Brixner, "Two-dimensional electronic spectroscopy can fully characterize the population transfer in molecular systems," J. Chem. Phys. **145**, 124312 (2016).
[27]A. Gelzinis, R. Augulis, V. Butkus, B. Robert, and L. Valkunas, "Two-dimensional spectroscopy for non-specialists," Biochim. Biophys. Acta, Bioenerg. **1860**, 271–285 (2019).
[28]R. D. Mehlenbacher, T. J. McDonough, M. Grechko, M.-Y. Wu, M. S. Arnold, and M. T. Zanni, "Energy transfer pathways in semiconducting carbon nanotubes revealed using two-dimensional white-light spectroscopy," Nat. Commun. **6**, 6732 (2015).
[29]N. M. Kearns, A. C. Jones, M. B. Kunz, R. T. Allen, J. T. Flach, and M. T. Zanni, "Two-dimensional white-light spectroscopy using supercontinuum from an all-normal dispersion photonic crystal fiber pumped by a 70 MHz Yb fiber oscillator," J. Phys. Chem. A **123**, 3046–3055 (2019).
[30]M. Th. Hassan, T. T. Luu, A. Moulet, O. Raskazovskaya, P. Zhokhov, M. Garg, N. Karpowicz, A. M. Zheltikov, V. Pervak, F. Krausz *et al.*, "Optical attosecond pulses and tracking the nonlinear response of bound electrons," Nature **530**, 66–70 (2016).
[31]Y. Song, A. Konar, R. Sechrist, V. P. Roy, R. Duan, J. Dziurgot, V. Policht, Y. A. Matutes, K. J. Kubarych, and J. P. Ogilvie, "Multispectral multidimensional spectrometer spanning the ultraviolet to the mid-infrared," Rev. Sci. Instrum. **90**, 013108 (2019).
[32]S. Mukamel, *Principles of Nonlinear Optical Spectroscopy* (Oxford University Press, 1995).
[33]S. Mukamel, "Multidimensional femtosecond correlation spectroscopies of electronic and vibrational excitations," Annu. Rev. Phys. Chem. **51**, 691–729 (2000).
[34]M. Cho, "Coherent two-dimensional optical spectroscopy," Chem. Rev. **108**, 1331–1418 (2008).
[35]S.-H. Shim and M. T. Zanni, "How to turn your pump–probe instrument into a multidimensional spectrometer: 2D IR and Vis spectroscopies *via* pulse shaping," Phys. Chem. Chem. Phys. **11**, 748–761 (2009).
[36]P. Hamm and M. T. Zanni, *Concepts and Methods of 2D Infrared Spectroscopy*, 1st ed. (Cambridge University Press, 2011).
[37]L. Valkunas, D. Abramavicius, and T. Mančal, *Molecular Excitation Dynamics and Relaxation* (Wiley-VCH, Weinheim, 2013).
[38]F. Šanda, V. Perlík, C. N. Lincoln, and J. Hauer, "Center line slope analysis in two-dimensional electronic spectroscopy," J. Phys. Chem. A **119**, 10893–10909 (2015).
[39]G. D. Scholes, "Quantum-coherent electronic energy transfer: Did nature think of it first?," J. Phys. Chem. Lett. **1**, 2–8 (2010).
[40]H.-G. Duan, V. I. Prokhorenko, R. J. Cogdell, K. Ashraf, A. L. Stevens, M. Thorwart, and R. J. D. Miller, "Nature does not rely on long-lived electronic quantum coherence for photosynthetic energy transfer," Proc. Natl. Acad. Sci. U. S. A. **114**, 8493–8498 (2017).
[41]V. Tiwari, W. K. Peters, and D. M. Jonas, "Electronic energy transfer through non-adiabatic vibrational-electronic resonance. I. Theory for a dimer," J. Chem. Phys. **147**, 154308 (2017).
[42]E. C. Wu, E. A. Arsenault, P. Bhattacharyya, N. H. C. Lewis, and G. R. Fleming, "Two-dimensional electronic vibrational spectroscopy and ultrafast excitonic and vibronic photosynthetic energy transfer," Faraday Discuss. **216**, 116–132 (2019).
[43]D. Polli, P. Altoè, O. Weingart, K. M. Spillane, C. Manzoni, D. Brida, G. Tomasello, G. Orlandi, P. Kukura, R. A. Mathies *et al.*, "Conical intersection dynamics of the primary photoisomerization event in vision," Nature **467**, 440–443 (2010).
[44]M. Liebel and P. Kukura, "Broad-band impulsive vibrational spectroscopy of excited electronic states in the time domain," J. Phys. Chem. Lett. **4**, 1358–1364 (2013).
[45]R. Monni, G. Capano, G. Auböck, H. B. Gray, A. Vlček, I. Tavernelli, and M. Chergui, "Vibrational coherence transfer in the ultrafast intersystem crossing of a diplatinum complex in solution," Proc. Natl. Acad. Sci. U. S. A. **115**, E6396–E6403 (2018).
[46]V. Butkus, L. Valkunas, and D. Abramavicius, "Molecular vibrations-induced quantum beats in two-dimensional electronic spectroscopy," J. Chem. Phys. **137**, 044513 (2012).
[47]J. C. Dean and G. D. Scholes, "Coherence spectroscopy in the condensed phase: Insights into molecular structure, environment, and interactions," Acc. Chem. Res. **50**, 2746–2755 (2017).
[48]P. Nuernberger, S. Ruetzel, and T. Brixner, "Multidimensional electronic spectroscopy of photochemical reactions," Angew. Chem., Int. Ed. **54**, 11368–11386 (2015).
[49]D. B. Turner, K. E. Wilk, P. M. G. Curmi, and G. D. Scholes, "Comparison of electronic and vibrational coherence measured by two-dimensional electronic spectroscopy," J. Phys. Chem. Lett. **2**, 1904–1911 (2011).
[50]V. Butkus, D. Zigmantas, L. Valkunas, and D. Abramavicius, "Vibrational vs. electronic coherences in 2D spectrum of molecular systems," Chem. Phys. Lett. **545**, 40–43 (2012).
[51]F. Ma and A. Yartsev, "Ultrafast photoisomerization of pinacyanol: Watching an excited state reaction transiting from barrier to barrierless forms," RSC Adv. **6**, 45210–45218 (2016).
[52]A. Al Haddad, A. Chauvet, J. Ojeda, C. Arrell, F. van Mourik, G. Auböck, and M. Chergui, "Set-up for broadband Fourier-transform multidimensional electronic spectroscopy," Opt. Lett. **40**, 312–315 (2015).
[53]M. Nisoli, S. Stagira, S. De Silvestri, O. Svelto, S. Sartania, Z. Cheng, M. Lenzner, C. Spielmann, and F. Krausz, "A novel-high energy pulse compression system: Generation of multigigawatt sub-5-fs pulses," Appl. Phys. B: Lasers Opt. **65**, 189–196 (1997).
[54]M. Schnürer, Z. Cheng, S. Sartania, M. Hentschel, G. Tempea, T. Brabec, and F. Krausz, "Guiding and high-harmonic generation of sub-10-fs pulses in hollow-core fibers at 10^{15} W/cm^2," Appl. Phys. B: Lasers Opt. **67**, 263–266 (1998).

[55]T. Witting, F. Frank, C. A. Arrell, W. A. Okell, J. P. Marangos, and J. W. G. Tisch, "Characterization of high-intensity sub-4-fs laser pulses using spatially encoded spectral shearing interferometry," Opt. Lett. **36**, 1680 (2011).
[56]T. Witting, F. Frank, W. A. Okell, C. A. Arrell, J. P. Marangos, and J. W. G. Tisch, "Sub-4-fs laser pulse characterization by spatially resolved spectral shearing interferometry and attosecond streaking," J. Phys. B: At., Mol. Opt. Phys. **45**, 074014 (2012).
[57]W. A. Okell, T. Witting, D. Fabris, D. Austin, M. Bocoum, F. Frank, A. Ricci, A. Jullien, D. Walke, J. P. Marangos *et al.*, "Carrier-envelope phase stability of hollow fibers used for high-energy few-cycle pulse generation," Opt. Lett. **38**, 3918 (2013).
[58]B. Alonso, M. Miranda, F. Silva, V. Pervak, J. Rauschenberger, J. San Román, Í. J. Sola, and H. Crespo, "Characterization of sub-two-cycle pulses from a hollow-core fiber compressor in the spatiotemporal and spatiospectral domains," Appl. Phys. B **112**, 105–114 (2013).
[59]L. Mewes, *Non-Equilibrium Dynamics of Di-Platinum Complexes and Molecular Dyes in Solution: Insights from Transient Absorption and Two-Dimensional Fourier Transform Spectroscopy* (EPFL, Lausanne, 2019).
[60]M. K. Yetzbacher, N. Belabas, K. A. Kitney, and D. M. Jonas, "Propagation, beam geometry, and detection distortions of peak shapes in two-dimensional Fourier transform spectra," J. Chem. Phys. **126**, 044511 (2007).
[61]R. Augulis and D. Zigmantas, "Detector and dispersive delay calibration issues in broadband 2D electronic spectroscopy," J. Opt. Soc. Am. B **30**, 1770 (2013).
[62]R. M. Mersereau and A. V. Oppenheim, "Digital reconstruction of multidimensional signals from their projections," Proc. IEEE **62**, 1319–1338 (1974).
[63]J. N. Sweetser, D. N. Fittinghoff, and R. Trebino, "Transient-grating frequency-resolved optical gating," Opt. Lett. **22**, 519–521 (1997).
[64]L. Wei and W. Min, "Electronic preresonance stimulated Raman scattering microscopy," J. Phys. Chem. Lett. **9**, 4294–4301 (2018).
[65]M. J. Frisch, G. W. Trucks, H. B. Schlegel, G. E. Scuseria, M. A. Robb, J. R. Cheeseman, G. Scalmani, V. Barone, G. A. Petersson, H. Nakatsuji *et al.*, Gaussian 16, Revision C.01, 2016.
[66]*NIST Computational Chemistry Comparison and Benchmark Database*, NIST Standard Reference Database Number 101 Release 21, edited by R. D. Johnson III, 2020.
[67]O. Bräm, "Ultrafast broadband fluorescence up-conversion study of the electronic relaxation of metalloporphyrins," J. Phys. Chem. A **8**, 1461 (2019).
[68]O. Bräm, F. Messina, A. M. El-Zohry, A. Cannizzo, and M. Chergui, "Polychromatic femtosecond fluorescence studies of metal–polypyridine complexes in solution," Chem. Phys. **393**, 51–57 (2012).
[69]A. Galestian Pour, C. N. Lincoln, V. Perlík, F. Šanda, and J. Hauer, "Anharmonic vibrational effects in linear and two-dimensional electronic spectra," Phys. Chem. Chem. Phys. **19**, 24752–24760 (2017).
[70]L. Mewes, MultidimensionalSpectroscopy.Jl, 2020.
[71]S. Krämer, D. Plankensteiner, L. Ostermann, and H. Ritsch, "QuantumOptics.jl: A Julia framework for simulating open quantum systems," Comput. Phys. Commun. **227**, 109–116 (2018).
[72]J. A. B. Ferreira and S. M. B. Costa, "Activationless nonradiative decay in rhodamines: Role of NH and lower frequency vibrations in solvent kinetic isotope effects," Chem. Phys. **321**, 197–208 (2006).
[73]E. Thyrhaug, S. Krause, A. Perri, G. Cerullo, D. Polli, T. Vosch, and J. Hauer, "Single-molecule excitation–emission spectroscopy," Proc. Natl. Acad. Sci. U. S. A. **116**, 4064–4069 (2019).
[74]P. Kukura, D. W. McCamant, and R. A. Mathies, "Femtosecond stimulated Raman spectroscopy," Annu. Rev. Phys. Chem. **58**, 461–488 (2007).
[75]N. Christensson, B. Dietzek, A. Yartsev, and T. Pullerits, "Electronic photon echo spectroscopy and vibrations," Vib. Spectrosc. **53**, 2–5 (2010).
[76]V. Sundstrom and T. Gillbro, "Transient absorption spectra of pinacyanol and cyanine photoisomers obtained with a sync-pumped picosecond dye laser and independently tunable probe light," Chem. Phys. Lett. **94**, 580–584 (1983).
[77]A. Yartsev, J.-L. Alvarez, U. Åberg, and V. Sundström, "Overdamped wavepacket motion along a barrierless potential energy surface in excited state isomerization," Chem. Phys. Lett. **243**, 281–289 (1995).
[78]W. Werncke, T. J. Tschol, H.-J. Weigmann, M. Pfeiffer, A. Lau, S. Rentsch, and A. Graness, "Photoisomerization studies of pinacyanol using nanosecond time-resolved resonance cars," J. Raman Spectrosc. **18**, 323–326 (1987).
[79]M. Hashimoto, T. Araki, and S. Kawata, "Molecular vibration imaging in the fingerprint region by use of coherent anti-Stokes Raman scattering microscopy with a collinear configuration," Opt. Lett. **25**, 1768 (2000).
[80]N. Dudovich, D. Oron, and Y. Silberberg, "Single-pulse coherent anti-Stokes Raman spectroscopy in the fingerprint spectral region," J. Chem. Phys. **118**, 9208–9215 (2003).
[81]W. W. Parson, *Modern Optical Spectroscopy*, 2nd ed. (Springer, 2015), ISBN: 978-3-662-46776-3.
[82]J.-P. Yang and R. H. Callender, "The resonance Raman spectra of some cyanine dyes," J. Raman Spectrosc. **16**, 319–321 (1985).
[83]J. Segarra-Martí, S. Mukamel, M. Garavelli, A. Nenov, and I. Rivalta, "Towards accurate simulation of two-dimensional electronic spectroscopy," Top. Curr. Chem. **376**, 24 (2018).
[84]T. Begušić and J. Vaníček, "On-the-fly *ab initio* semiclassical evaluation of third-order response functions for two-dimensional electronic spectroscopy," J. Chem. Phys. **153**, 184110 (2020).
[85]I. Conti, G. Cerullo, A. Nenov, and M. Garavelli, "Ultrafast spectroscopy of photoactive molecular systems from first principles: Where we stand today and where we are going," J. Am. Chem. Soc. **23**, 16117 (2020).
[86]M. K. Lawless and R. A. Mathies, "Excited-state structure and electronic dephasing time of nile blue from absolute resonance Raman intensities," J. Chem. Phys. **96**, 8037–8045 (1992).
[87]M. H. Stockett, J. Houmøller, and S. Brøndsted Nielsen, "Nile blue shows its true colors in gas-phase absorption and luminescence ion spectroscopy," J. Chem. Phys. **145**, 104303 (2016).
[88]H. L. Fragnito, J.-Y. Bigot, P. C. Becker, and C. V. Shank, "Evolution of the vibronic absorption spectrum in a molecule following impulsive excitation with a 6 fs optical pulse," Chem. Phys. Lett. **160**, 101 (1989).
[89]W. T. Pollard, H. L. Fragnito, J.-Y. Bigot, C. V. Shank, and R. A. Mathies, "Quantum-mechanical theory for 6 fs dynamic absorption spectroscopy and its application to nile blue," Chem. Phys. Lett. **168**, 239–245 (1990).
[90]J. Hauer, T. Buckup, and M. Motzkus, "Enhancement of molecular modes by electronically resonant multipulse excitation: Further progress towards mode selective chemistry," J. Chem. Phys. **125**, 061101 (2006).
[91]D. Egorova, M. F. Gelin, and W. Domcke, "Analysis of cross peaks in two-dimensional electronic photon-echo spectroscopy for simple models with vibrations and dissipation," J. Chem. Phys. **126**, 074314 (2007).
[92]A. Reigue, B. Auguié, P. G. Etchegoin, and E. C. Le Ru, "CW measurements of resonance Raman profiles, line-widths, and cross-sections of fluorescent dyes: Application to nile blue A in water and ethanol: Measuring resonance Raman spectra of fluorophores," J. Raman Spectrosc. **44**, 573–581 (2013).
[93]B. Dietzek, N. Christensson, P. Kjellberg, T. Pascher, T. Pullerits, and A. Yartsev, "Appearance of intramolecular high-frequency vibrations in two-dimensional, time-integrated three-pulse photon echo data," Phys. Chem. Chem. Phys. **9**, 701–710 (2007).
[94]S. Malkmus, R. Dürr, C. Sobotta, H. Pulvermacher, W. Zinth, and M. Braun, "Chirp dependence of wave packet motion in oxazine 1," J. Phys. Chem. A **109**, 10488–10492 (2005).
[95]T. J. Quincy, M. S. Barclay, M. Caricato, and C. G. Elles, "Probing dynamics in higher-lying electronic states with resonance-enhanced femtosecond stimulated Raman spectroscopy," J. Phys. Chem. A **122**, 8308–8319 (2018).
[96]Y. Nagasawa, A. Watanabe, H. Takikawa, and T. Okada, "Solute dependence of three pulse photon echo peak shift measurements in methanol solution," J. Phys. Chem. A **107**, 632–641 (2003).
[97]M. Marazzi, H. Gattuso, and A. Monari, "Nile blue and nile red optical properties predicted by TD-DFT and CASPT2 methods: Static and dynamic solvent effects," Theor. Chem. Acc. **135**, 57 (2016).
[98]H. Sato, M. Kawasaki, K. Kasatani, and M.-a. Katsumata, "Raman spectra of some indo-, thia- and selena-carbocyanine dyes," J. Raman Spectrosc. **19**, 129–132 (1988).

[99]B. Spokoyny, C. J. Koh, and E. Harel, "Stable and high-power few cycle supercontinuum for 2D ultrabroadband electronic spectroscopy," Opt. Lett. **40**, 1014 (2015).
[100]X. Ma, J. Dostál, and T. Brixner, "Broadband 7-fs diffractive-optic-based 2D electronic spectroscopy using hollow-core fiber compression," Opt. Express **24**, 20781 (2016).
[101]L. A. Bizimana, J. Brazard, W. P. Carbery, T. Gellen, and D. B. Turner, "Resolving molecular vibronic structure using high-sensitivity two-dimensional electronic spectroscopy," J. Chem. Phys. **143**, 164203 (2015).
[102]M. Son, S. Mosquera-Vázquez, and G. S. Schlau-Cohen, "Ultrabroadband 2D electronic spectroscopy with high-speed, shot-to-shot detection," Opt. Express **25**, 18950 (2017).
[103]N. M. Kearns, R. D. Mehlenbacher, A. C. Jones, and M. T. Zanni, "Broadband 2D electronic spectrometer using white light and pulse shaping: Noise and signal evaluation at 1 and 100 kHz," Opt. Express **25**, 7869 (2017).
[104]N. Krebs, I. Pugliesi, J. Hauer, and E. Riedle, "Two-dimensional Fourier transform spectroscopy in the ultraviolet with sub-20 fs pump pulses and 250–720 Nm supercontinuum probe," New J. Phys. **15**, 085016 (2013).
[105]R. B. Varillas, A. Candeo, D. Viola, M. Garavelli, S. De Silvestri, G. Cerullo, and C. Manzoni, "Microjoule-level, tunable sub-10 fs UV pulses by broadband sum-frequency generation," Opt. Lett. **39**, 3849 (2014).
[106]R. Borrego-Varillas, A. Oriana, L. Ganzer, A. Trifonov, I. Buchvarov, C. Manzoni, and G. Cerullo, "Two-dimensional electronic spectroscopy in the ultraviolet by a birefringent delay line," Opt. Express **24**, 28491 (2016).